Hindawi Publishing Corporation
Advances in Optical Technologies
Volume 2012, Article ID 976868, 8 pages
doi:10.1155/2012/976868

*Research Article*

# Fabrication and Evaluation of Large Area Mo/Si Soft X-Ray Multilayer Mirrors at Indus SR Facilities

**P. N. Rao, Maheswar Nayak, G. S. Lodha, S. K. Rai, A. K. Srivastava, M. H. Modi, and A. Sagdeo**

*X-ray Optics Section, Indus Synchrotrons Utilization Division, Raja Ramanna Centre for Advanced Technology, Indore-452013, India*

Correspondence should be addressed to Maheswar Nayak, mnayak@rrcat.gov.in

Received 30 April 2012; Accepted 6 July 2012

Academic Editor: Yong Zhao



Large area Mo/Si multilayer (ML) mirrors with high reflectivity are fabricated using magnetron sputtering deposition system. Thin film growth is optimized for film roughness, density, and interface quality by changing process parameters through fabrication of thin films. Mo/Si MLs are fabricated with varying thickness ratio, number of layer pairs, and periodicity from 0.3 to 0.45, 5 to 65, and 40 to 100 Å, respectively. The samples are characterized using hard X-ray reflectivity and transmission electron microscopy. Soft X-ray performance tests of MLs are done by soft X-ray reflectivity using Indus-1 synchrotron radiation. ML coating with thickness errors of ~0.03% per layer and interface roughness in the range of 2 to 5 Å has been realized. The lateral variation of the periodicity is controlled within 0.5 Å over the $300 \times 100\,\text{mm}^2$ area of the plane substrate by using substrate motion and appropriate masking arrangement. Maximum variation of periodicity from run to run is less than 0.5 Å. Peak reflectivity of ~63% at wavelength of ~127 Å is achieved for incident angle of 71 degree.

## 1. Introduction

X-ray multilayer (ML) mirror is a one dimensional artificial Bragg reflector [1]. It bridges between naturally occurring crystal optics and total reflection optics. The former gives excellent energy resolution however integrated reflectivity is small because of narrow rocking curve. The later gives high reflectivity at extremely small glancing incidence geometry and acts as energy cutoff reflector. X-ray ML mirror provides high integrated reflectivity with moderate spectral bandpass. ML mirror has reasonable high acceptance angle compared to total reflection optics in hard X-ray region, and also gives normal incidence optics in soft X-ray /extreme ultra violet spectral range. The main advantages of ML mirrors stem from the tunability of period thickness, composition, lateral and in-depth gradient of periodicity; these can be tailored according to the desired incidence geometry and wavelength regime. Furthermore, ML mirrors have the advantage of being used for focusing and imaging applications by depositing structures on figured surface. However, fabrication of these ML mirrors is a challenging task. It requires deposition system capable of fabricating uniform, ultrathin smooth layer (~8 to 50 Å) with thickness control on atomic scale, and number of layer pairs ranging from ~50 to 500. This task becomes more stringent in case of large area ML for device applications.

Large area MLs have different potential applications such as soft X-ray/extreme ultra violet (EUV) lithography [2–5], soft X-ray imaging using Schwarzschild objective [6], double ML monochromator [7–9], super mirror for hard X-ray synchrotron, astrophysics [10], X-ray telescope [11, 12], and generating parallel/focusing X-ray beam using Göbel mirrors [13, 14]. For optical system using more than one ML mirror, the layer-to-layer thickness, uniformity, and run-to-run reproducibility during fabrication of these ML mirrors should be precisely controlled. Achieving high reflectivity, run-to-run stability, and uniformity over large area require: (i) a stable and reproducible fabrication system following (ii) precise geometrical configuration of the fabrication system along with proper masking arrangements for improvement in uniformity; (iii) optimization of process parameters, such as rate of deposition, kinetic energy of add-atoms, and so forth to obtain optimum thin film growth condition. Various techniques have been attempted by different groups

to produce large area ML mirrors on flat as well as figured substrates.

Using magnetron sputtering, Kortright et al. [6] obtained thickness uniformity better than 99% on 75-mm diameter flat substrate through substrate spinning and masking. Takenaka et al. [3] achieved uniformity of 99.2% on 6-inch diameter flat substrate with 63% reflectivity at 130 Å for Mo/Si MLs fabricated by RF magnetron sputtering through substrate spinning and masking. MacKay et al. [8] and Tsuruta et al. [15] fabricated MLs on flat silicon substrate using magnetron sputtering for monochromator application. The former have obtained uniformity >99% on $75 \times 25\,mm^2$ area, in W/C ML, using substrate rotation and masking, whereas the latter have obtained uniformity 99% on $152 \times 38\,mm^2$ area in Mo/C ML using substrate rotation. As the dimension of optics increases further, additional constraints are imposed in deposition system to generate stable and uniform distribution of plasma for thickness control. Few reports are available to fabricate MLs with increased dimension. Dietsch et al. [16] fabricated Ni/C MLs on 6-inch diameter substrate (both flat and curved) by pulse laser deposition method. By using substrate motion and masking, they have obtained uniformity 99% with layer-to-layer thickness error ≤0.1 Å and run-to-run stability <0.5 Å. Gawlitza et al. [14] have fabricated Mo/Si MLs on 200 mm diameter flat substrate using ion beam deposition with ion assist gun. Using mask and substrate rotation they obtained uniformity 99.9% up to radius of 80 mm; after that uniformity decreases to 99.7%. Recently Morawe et al. [9] fabricated W/$B_4$C ML on float glass substrate and achieved uniformity ~99.5% over an area of $1200 \times 200\,mm^2$ using substrate motion and masking arrangements.

To meet these requirements, recently we have commissioned a specially designed magnetron sputtering system. In this paper we report fabrication and evaluation of high reflectivity Mo/Si MLs on $300 \times 100\,mm^2$ area substrate with good control over layer-to-layer thickness, lateral thickness homogeneity, and run-to-run reproducibility. We have achieved high-quality interface structure by optimizing process parameters.

## 2. Experimental

ML samples are fabricated using magnetron sputtering system which has both DC and RF compatibility [17]. There are two rectangular cathodes of size 500 mm × 100 mm each. The sputtering process is in a horizontal configuration. Sample movement is fully software controlled from load lock to main processing chamber. The base pressure in main chamber and load lock system is $1 \times 10^{-8}$ mbar and$8 \times 10^{-8}$ mbar, respectively. Load lock chamber contains an RF ion etcher for substrate cleaning. All test samples are fabricated on Si and float glass substrates. Substrate moves linearly over sputter sources with variable speed. The deposited material thickness is determined by the time of substrate exposure to the source, which, in turn depends on the velocity of the substrate. Purity of Mo and Si target is 99.9% and 99.99%, respectively. High purity (99.999%) argon is used as sputtering gas. DC power is used for sputtering of Mo and RF power is used for Si. During optimization of the sputtering parameters, sputtering power for Mo and Si is varied from 100 to 200 W and 200 to 400 W, respectively. Ar flow is varied from 4 to 12 sccm, resulting in pressure variation of the process chamber between $1.0 \times 10^{-3}$ to $8 \times 10^{-3}$ mbar. The target-substrate distance is varied from 50 mm to 150 mm. A reproducibility of target-substrate position of less than 0.5 mm is realized. During fabrication of MLs, ML periodicity (d) is varied from 40 to 100 Å, thickness ratio (ratio of Mo thickness to period thickness) (Γ) is varied from 0.3 to 0.45, and number of layer pairs (N) is varied from 5 to 65.

The performance of Mo/Si ML is tested using Indus-1 reflectivity beamline [18]. The beamline delivers radiation in the range of 40–1000 Å with high flux and moderate spectral resolution using a toroidal grating monochromator. Various absorption edge filters are provided in the beamline to suppress the higher-order contamination from monochromator. The present reflectance measurements are carried out in the s-polarized geometry. The wavelength resolution $\lambda/\Delta\lambda$ of beam line in this spectral region is 200–500. The detector used is EUV/soft X-ray photo diode. Hard X-ray reflectivity (XRR) measurements are performed on Bruker Discover D8 diffractometer. Transmission electron microscope (TEM) investigations are carried out on a Philips CM 200 TEM, operated at 200 kV accelerating voltage. The microscope is used in imaging, diffraction, and analytical modes.

## 3. Results and Discussion

*3.1. Layer Structure and Thickness Control.* Fabrication of high-reflectivity MLs with good energy band pass depends strongly on nature of interface, density contrast, and thickness error. While thickness error from layer to layer in the multilayer stacks depend on the stability of the process parameters, the interface characteristics and density contrast depends on kinetic energy (KE) of the add- atoms. KE of condensed particles is optimized by adjusting flux and energies of sputtered atoms through a systematic variation of process parameters during growth of thin films, bilayers, and finally MLs. Desired film quality is obtained after several iterations, by optimizing gas flow rate, pressure, power, target- substrate distance, and substrate speed. Some of these results are discussed below.

A typical example of the influence of argon pressure and film thickness on the quality of Mo single film is shown in Figure 1. Measured XRR profile is fitted using Parratt formalism [19]. For fitting, a low-density Mo oxide layer of thickness ~45 Å is assumed at the top of Mo thin films. The best fit results reveals that the rms surface roughness of oxide layer is in the range of 8 Å for samples Mo-1, Mo-2, Mo-3, and Mo-6 whereas 5 Å for samples Mo-4 and Mo-5. The substrate roughness of 4 Å is assumed in fitting of all samples. The film thickness, surface roughness, and mass density obtained from the best-fit to measured XRR data are shown in Table 1. The roughness of film increases with increasing thickness and for same thickness, roughness

Table 1: Mo film quality interms of thickness ($t$), roughness ($\sigma$) and density ($\rho$), as a function of argon pressure obtained from the best-fit XRR results of Figure 1.

| Film | $P$ (mbar) | $t$ (Å) | $\sigma$ (Å) | $\rho$ (gm/cc) |
|---|---|---|---|---|
| Mo-1 | $4.0 \times 10^{-3}$ | 87.5 | 4 | 7.07 |
| Mo-2 | $4.0 \times 10^{-3}$ | 116 | 4.5 | 10.06 |
| Mo-3 | $4.0 \times 10^{-3}$ | 180 | 6 | 10.1 |
| Mo-4 | $3 \times 10^{-3}$ | 155 | 3 | 10.2 |
| M0-5 | $5 \times 10^{-3}$ | 160 | 6.5 | 9.79 |
| Mo-6 | $8 \times 10^{-3}$ | 175 | 8 | 8.86 |

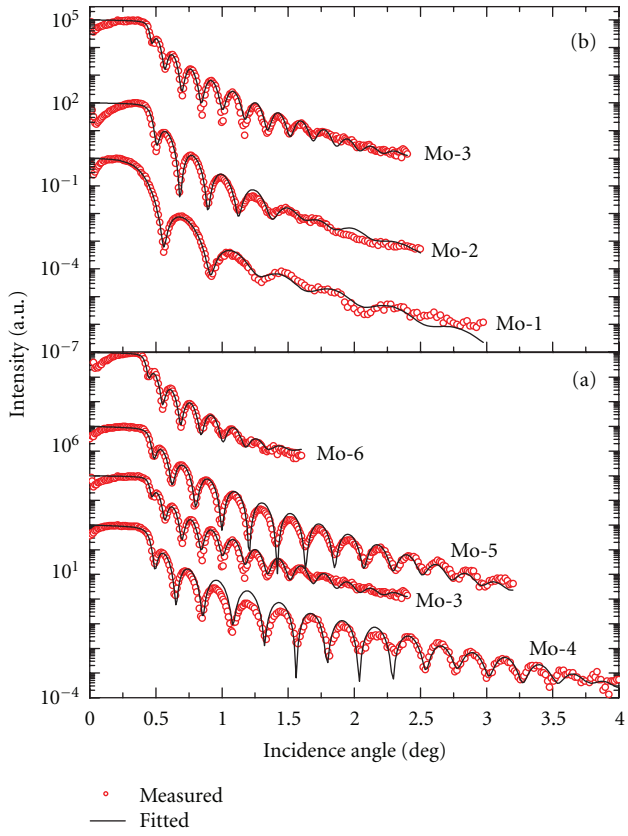


Figure 1: Measured and fitted XRR profile at Cu $K_\alpha$ wavelength ($\lambda$ = 1.54 Å) for Mo thin films. (a) as a function of Ar pressure (b) as a function of Mo thickness at constant Ar pressure. The best fit results are given in Table 1.

increases with increasing pressure. Previously it was observed that with increase in working pressure, the growth pattern of sputtered films changes from compact structure to a columnar structure [2, 20, 21]. The increase in roughness of film at higher gas pressure is attributed to decrease in surface energy of add-atoms during film growth. Similarly, the influence of power, target-substrate distance, and so forth are examined on the film quality. To realize good interface, the process parameters are optimized for both Mo and Si. In case of Si film, process parameters are optimized by fabricating Si-on-Mo bilayer. The rate of deposition is maintained at 3 Å/s and 0.4 Å/s for Mo and Si, respectively, at working pressure $3 \times 10^{-3}$ mbar with 7 sccm gas flow rate. For above working pressure, the optimized sputtering power for Mo and Si is 150 W and 300 W, respectively. These powers provide optimized activation energy to the deposited atoms for surface diffusion enabling growth of smooth films. Subsequently the morphology of the film is adjusted by varying geometrical parameters such as motion of substrate. Optimized substrate motion over the target for Mo is 9.2 mm/s and that of Si is 1.34 mm/s.

A challenging task during fabrication of ML stacks is to achieve a stable deposition condition for precise control of thickness in atomic scale from layer to layer. This needs that discharge plasma and its distribution over the target should be stable during fabrication of ML, which takes approximately few hours. The key parameters for stable and uniform plasma depend on purity of Ar gas, uniform gas flow over the target, conditioning of vacuum chamber (degassing and quality of vacuum), and a stable plasma power supply. Quality of vacuum in the process chamber is maintained by constantly pumping without breaking vacuum in the chamber. The out-gassing from inner wall of process chamber was pre-conditioned by fabricating test samples for many runs before final fabrication of actual samples. For stable plasma and to avoid contamination from target surface during film growth before fabrications of actual ML samples, the target is presputtered for about 30 minutes. The stabilization of gas flow rate, power, and vacuum is maintained within $\pm 0.01$ sccm, $\pm 0.5$ W and $\pm 0.02 \times 10^{-3}$ mbar, respectively during the deposition process. For the determination of layer structure, intentionally, we fabricated multilayer samples with lower number of layer pairs for clarity in Kiessig oscillation between higher order Bragg peaks in the X-ray reflectivity pattern. Figure 2 shows a case study of two Mo/Si MLs with $N = 10$ but different periodicity. The successive higher order Bragg peaks reveal good quality of ML structure. The best-fit results are shown in Table 2. For ML-1, the measured full width at half maxima (FWHM) of 1st-order Bragg peak is $\Delta q_z = 0.0114$ Å$^{-1}$ which is close to the FWHM of ideal ML structure $\Delta q_z = 0.0111$ Å$^{-1}$. Similarly for ML-2, the measured FWHM of 1st order Bragg peak is $\Delta q_z = 0.0116$ Å$^{-1}$ which is also close to FWHM of real ML structure $\Delta q_z = 0.0114$ Å$^{-1}$. The best-fit results reveal high contrast in density between Mo and Si with interfacial roughness in the range of 2 to 4 Å. There is a presence of interlayer (IL) in between Mo and Si, which is asymmetric in thickness.

After optimizing process parameters by fabricating smaller number of layer pairs, MLs are fabricated with larger number of layer pairs. Figure 3 shows the measured and fitted XRR profile of two Mo/Si MLs. ML-3 has $N = 65$ and periodicity $d$ = 68 Å whereas ML-4 has $N = 60$ and $d$ = 93.4 Å. Figure 3 shows that well-defined successive higher order Bragg peaks indicate good quality of ML structure in terms of roughness, thickness error, and density contrast. A calculated thickness error of ~0.03% per layer is obtained from higher order peak broadening. The best-fit results are shown in Table 2. XRR profile is fitted using four-layer model taking account of interlayer formation at the both

Table 2: Thickness and roughness of the various layers of Mo/Si MLs deduced from the fit of XRR results of Figures 2 and 3. IL1stands for interlayer at the Mo-on-Si interface, IL2 stands for interlayer at the Si-on-Mo interface. $\delta$ is the unit decrement of real part of the refractive index.

| Sample | Total thickness (Å) | Mo thickness (Å)<br>IL1 thickness (Å)<br>Si thickness (Å)<br>IL2 thickness (Å) | $\delta$Mo ($\times 10^{-6}$)<br>$\delta$IL1 ($\times 10^{-6}$)<br>$\delta$Si ($\times 10^{-6}$)<br>$\delta$IL2 ($\times 10^{-6}$) | Mo roughness (Å)<br>IL1 roughness (Å)<br>Si roughness (Å)<br>IL2 roughness (Å) |
|---|---|---|---|---|
| ML-1 | 90.3 | 28.0<br>8.9<br>47.4<br>6.0 | 26.0<br>9.5<br>6.04<br>22.8 | 4.7<br>3<br>4<br>2 |
| ML-2 | 66.0 | 16.7<br>8.0<br>35.0<br>6.3 | 26.0<br>9.54<br>6.0<br>23.8 | 4.7<br>3<br>4<br>2 |
| ML-3 | 68 | 21.0<br>9.0<br>31.0<br>7.0 | 28.0<br>9.5<br>7.6<br>18.5 | 5<br>4<br>4<br>2 |
| ML-4 | 93.4 | 30.4<br>10.0<br>44.5<br>8.5 | 28.02<br>6.55<br>8.0<br>14.5 | 5<br>4<br>4<br>3 |

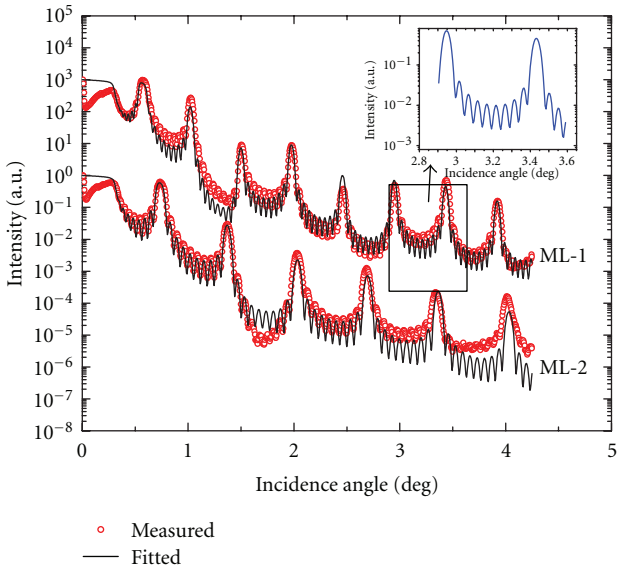


Figure 2: Measured and fitted XRR profile at Cu $K_\alpha$ wavelength ($\lambda$ = 1.54 Å) for Mo/Si MLs with $N = 10$ and with different periodicity. $d$ = 90 Å for ML-1 and $d$ = 66 Å for ML-2. The best fit results are given in Table 2.

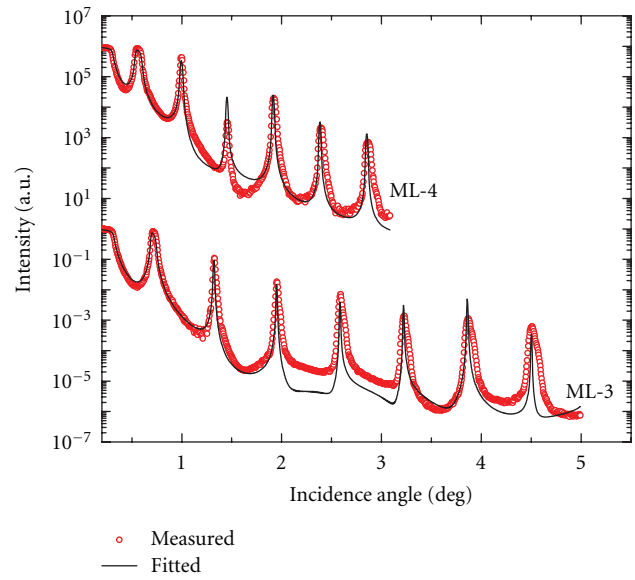


Figure 3: Measured and fitted XRR profile at Cu $K_\alpha$ wavelength ($\lambda$ = 1.54 Å) for Mo/Si MLs. ML-3 has $N = 65$ and $d$ = 68 Å and ML-4 has $N = 60$ and $d$ = 93.4 Å. The best fit results are given in Table 2.

interfaces, namely Mo-on-Si and Si-on-Mo. The interlayer arises because of inter diffusion/compound formation at the interfaces of Mo/Si system, which is commonly observed for Mo-Si system [22].

Cross-sectional electron microscopy studies are undertaken to study the interfaces and periodicity of Mo/Si ML. Figure 4 shows cross-sectional TEM micrograph of Mo/Si ML-3 with $N = 65$ layer pairs. The dark and light bands correspond to Mo and Si layers, respectively. Molybdenum has a higher atomic number ($Z = 42$) and therefore appears darker as it scatters more electrons than does silicon ($Z = 14$). ML shows a well-defined periodic structure with sharp

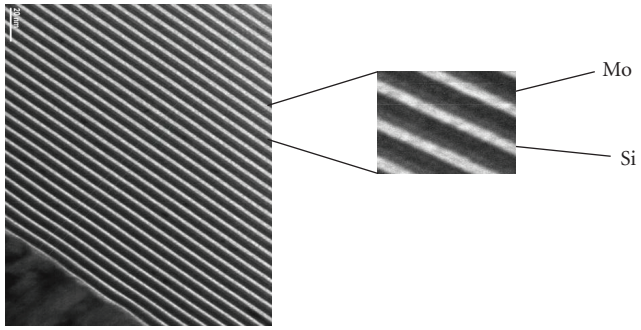


Figure 4: Cross-sectional TEM image of sample ML-3. Dark lines correspond to Mo and bright lines to Si.

interface. However, very thin asymmetric interlayers are observed in the zoomed region.

*3.2. Lateral Uniformity and Reproducibility.* Desired lateral thickness profile of the coating on large area substrate is obtained by iterative control of pumping port opening, argon flow from two sides of chamber, substrate motion, installation of masking arrangements, and optimization of target-substrate distance. Uniform flow of argon across the target is realized by flowing unequal gas flow rate on two sides of targets (along length) and adjusting opening of pumping port. Gas flow rate is higher on the pumping side than the other side, to compensate direct pumping effect. After assuring uniform gas flow, the spatial distribution of sputtered atoms depends upon the geometry of target and target-substrate distance. A planner rectangular magnetron source produces a rectangular-shaped sputtering track. More material is sputtered out from the target where magnetic field is more. The spatial distribution of deposition rate profile over a planner rectangular cathode is cosine like structure [23]. The deposition rate is more at centre and decreases systematically at both sides along the length. Furthermore, the spatial distribution of deposited flux is strongly dependent on target-substrate distance. As the target-substrate distance increases, the spatial distribution profile becomes uniform over the length of the target. However, as the target-substrate distance increases the deposition rate decreases. Furthermore, the film quality is affected if target-substrate distance is large. There is a trade-off between target-substrate distance which in turn depends on uniformity and deposition rate, as well as film quality. Thus, the strategy for controlling uniformity over length of target is to use appropriate masking geometry and to optimize target-substrate distance. For the present system, we have optimized target-substrate distance as 70 mm. To average out spatially variation of deposition rate along length of target, we employed different masking arrangements. To evaluate the lateral uniformity of periodicity, initially multilayers are fabricated on small substrates (size $2 \times 3\,\text{cm}^2$) placed at different positions over the area $300 \times 100\,\text{mm}^2$. Finally, the actual large-size multilayers are fabricated on float glass with size $300 \times 100\,\text{mm}^2$. Figure 5 shows measured reflectivity profile of Mo/Si ML at different positions along the length of

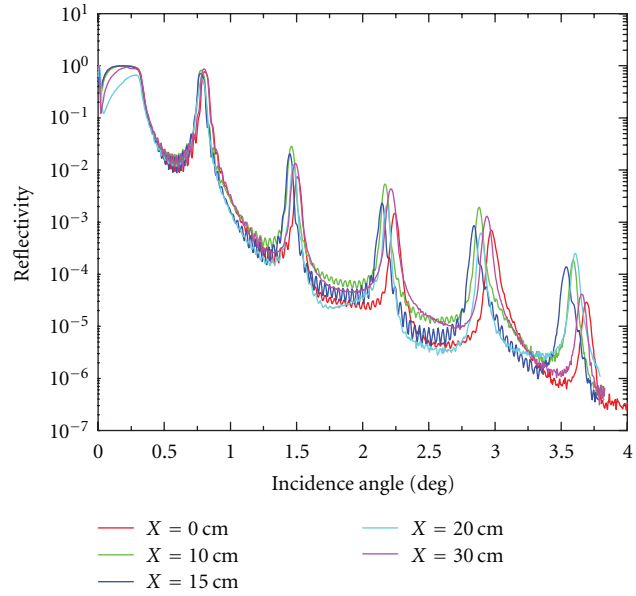


Figure 5: XRR profile of Mo/Si MLs with $N = 20$, $\Gamma = 0.35$ and $d = 62$ Å by placing substrates at different positions (X) along the length of the substrate holder and putting a rectangular mask.

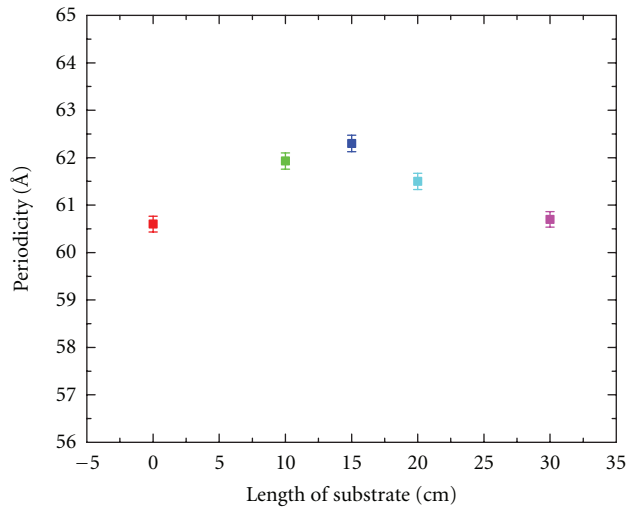


Figure 6: Measured lateral variation of periodicity along the length obtained from best-fit results of Figure 5.

substrate which are fabricated using a rectangular masking arrangement in between target and substrate. Figure 6 shows the periodicity of fabricated multilayer versus distances along the length of target which are obtained from best-fit XRR measurements. In Figure 6, it is evident that there is systematic decrease in periodicity in both sides along the length with respect to centre of substrate. This is due to decrease in deposition rate from centre to side along the length of target. The maximum variation in periodicity is ($\Delta d$) 1.7 Å.

In order to further minimize spatially variation of deposition rate along the length, we figured the mask, with

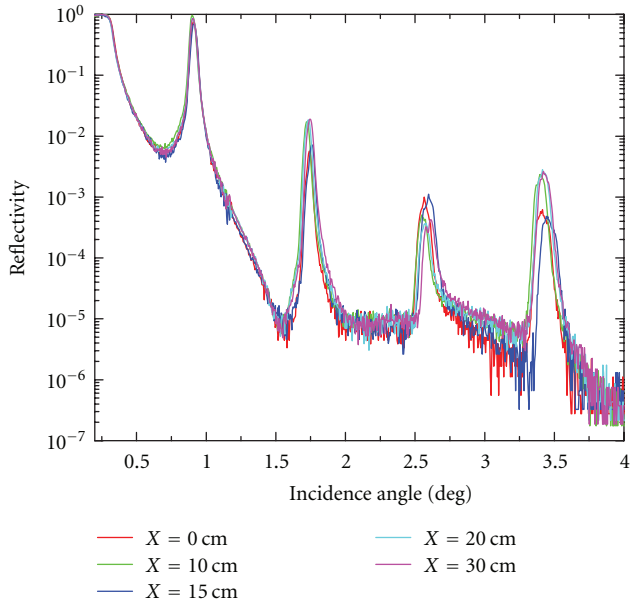


Figure 7: XRR spectra of Mo/Si MLs with $N = 65$, $\Gamma = 0.45$, and $d = 52$ Å by placing substrates at different positions (X) along the length of the substrate holder and using a mask with tapering towards center of target.

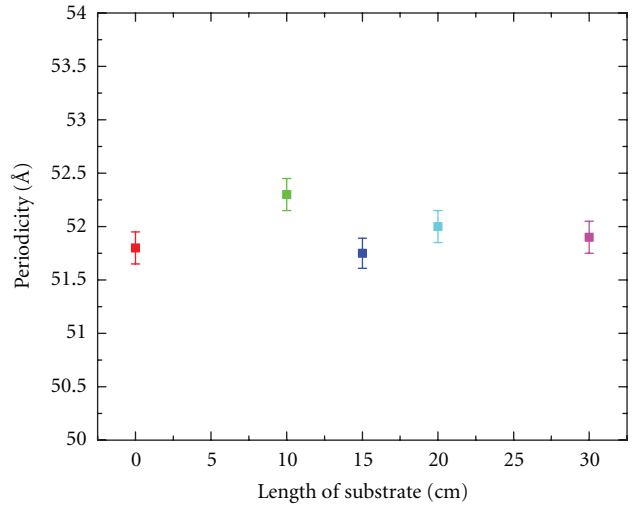


Figure 8: Measured lateral variation of periodicity along the length obtained from best-fit results of Figure 7.

tapering towards centre. More flux of deposited material at the centre compared to both sides is compensated by adjusting amount of tapering of mask towards centre. Figure 7 shows the measured reflectivity profile of Mo/Si MLs at different positions along the length of substrate which are fabricated using a modified masking arrangement with tapering towards centre. The corresponding variation in lateral periodicity which is obtained from the best-fit data is shown in Figure 8.The maximum lateral variation in periodicity is within 0.5 Å along 300 mm length of target. Furthermore, the linear motion of the substrate across the

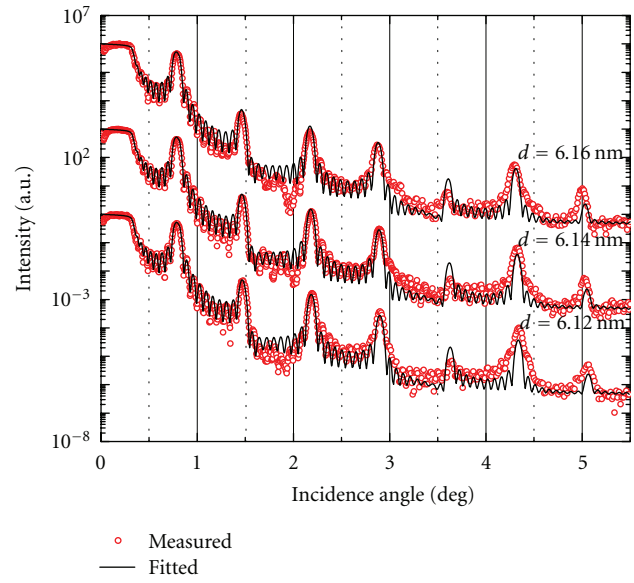


Figure 9: XRR spectra of Mo/Si MLs with $N = 10$, and $d = 61$ Å deposited from run-to-run under identical experimental conditions.

full opening of mask averages out the spatial variation of the deposition rate in the motion direction (i.e., along the width of target). In our present deposition system, the maximum width of sample is 100 mm. This limitation in sample width is to avoid cross talk between the targets during deposition.

Reproducibility is the crucial issue for larger-area multilayer for device applications. Our preconditioned system ensures reproducibility of system in terms of density contrast, interface quality, and thickness control from run to run. A typical example of reproducibility of fabricated multilayers from run to run is shown in Figure 9. Here, we show three different deposition runs keeping number of layer pair fixed at $N = 10$. The identical critical angle and similar reflectivity of 1st order Bragg peak of three samples indicate insignificant variation in film density. The best-fit results reveal identical interface quality for all the samples. Moreover, best-fit results reveal the variation in periodicity from run to run is better than 0.5 Å.

*3.3. Soft X-Ray Performance.* The actual performance of MLs is tested using reflectivity beam line on Indus-1 SR source. Figure 10 shows the angle versus reflectivity scan of ML-3 with $d = 68$ Å and $N = 65$ layer pairs at a wavelength of 127 Å. The ML has 63% peak reflectivity at an incidence angle of 71°. In inset, wavelength versus reflectivity scan measured at a Bragg angle of 72.5° is presented. The ML with suitable varying periodicity will be used for potential application in the wavelength range of 126–150 Å. The 63% of reflectivity obtained is comparable with 69% peak reflectance reported on standard Mo/Si system [24]. The spectral width of ML-3 is 2.3 eV. Mo/Si ML would be used as a polarizer and analyzer in soft X-ray region because of high throughput and polarizing power. Figure 11 shows the angle versus reflectivity scan of ML-4 which is designed to use as a polarizing element at

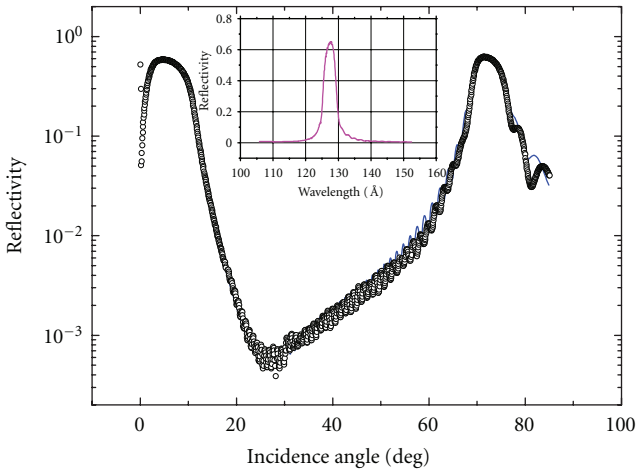


Figure 10: Measured and fitted soft X-ray reflectivity (angle scan) profile of Mo/Si ML (sample no. ML-3) at the wavelength $\lambda$ = 127 Å using synchrotron radiation. Inset shows wavelength versus reflectivity curve measured at angle of incidence of 72.5°.

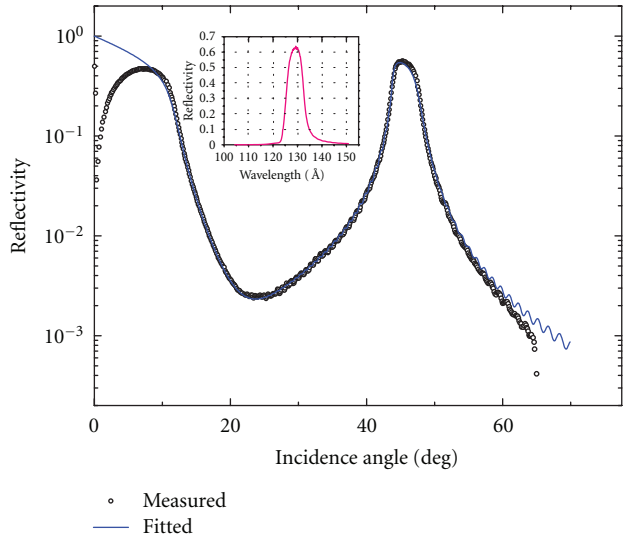


Figure 11: Measured and fitted of soft X-ray reflectivity profile of Mo/Si ML (sample no. ML-4) at the wavelength $\lambda$ = 130 Å using synchrotron radiation. Inset shows wavelength versus reflectivity curve measured at angle of incidence 45°.

wavelength of 130 Å with $d$ = 93.4 Å and $N$ = 60 layer pairs. This sample has Bragg peak at quasi-Brewster angle 45° at wavelength of 130 Å. The spectral width of ML-4 is 5.36 eV. In sample ML-4 numbers of layer pairs are optimized to get maximum s-reflectance to p-reflectance ratio.

## 4. Conclusions

Large area, high-reflectivity Mo/Si MLs are developed using specially designed magnetron sputtering system. The process parameters are optimized for growth of thin film suitable for X-ray ML fabrication. Mo/Si MLs are fabricated with rms interface roughness in the range of 2 to 5 Å. The lateral variation in periodicity of ML is minimized to 0.5 Å over 300 × 100 mm$^2$ area by proper masking arrangement, substrate motion, and choosing appropriate system configuration. The run-to-run variation in periodicity and thickness errors are less than 0.5 Å and 0.03% per layer, respectively. Reflectivity of more than 60% is routinely achieved at the wavelength above the silicon L-edge (~124 Å).

## References

[1] E. Spiller, *Soft X-Ray Optics*, SPIE, Bellingham, Wash, USA, 1994.

[2] D. G. Stearns, R. S. Rosen, and S. P. Vernon, "Multilayer mirror technology for soft-X-ray projection lithography," *Applied Optics*, vol. 32, no. 34, pp. 6952–6960, 1993.

[3] H. Takenaka, T. Kawamura, T. Haga, H. Kinoshita, and Y. Ishii, "Evaluation of large-area Mo/Si multilayer soft X-ray mirrors fabricated by RF magnetron sputtering," *Japanese Journal of Applied Physics, Part 1*, vol. 34, no. 9 A, pp. 5027–5031, 1995.

[4] D. L. Windit and W. K. Waskiewicz, "Multilayer facilities required for extreme-ultraviolet lithography," *Journal of Vacuum Science and Technology B*, vol. 12, no. 6, pp. 3826–3832, 1994.

[5] C. Montcalm, R. F. Grabner, R. M. Hudyma et al., "Atomic-precision multilayer coating of the first set of optics for an extreme-ultraviolet lithography prototype system," *Applied Optics*, vol. 41, no. 16, pp. 3262–3269, 2002.

[6] J. B. Kortright, E. M. Gullikson, and P. E. Denham, "Masked deposition techniques for achieving multilayer period variations required for short-wavelength (68-Å) soft-X-ray imaging optics," *Applied Optics*, vol. 32, no. 34, pp. 6961–6968, 1993.

[7] C. K. Malek, T. Moreno, R. Barchewitz, R. Rivoira, and Y. Lepêtre, "Performances of large multilayer mirrors for the 0.5–1.5 nm range," *Review of Scientific Instruments*, vol. 63, no. 9, pp. 4102–4107, 1992.

[8] J. F. MacKay, D. W. Pearson, B. E. Nelms, P. M. DeLuca Jr., M. N. Gould, and M. G. Lagally, "A double mirror W/C multilayer monochromator for radiation biology applications," *Medical Physics*, vol. 25, no. 5, pp. 773–779, 1998.

[9] Ch. Morawe and J. C. Peffen, "Thickness control of large area X-ray multilayers," in *Advances in X-Ray/EUV Optics and Components IV*, vol. 7448 of *Proceedings of SPIE*, San Diego, Calif, USA, August 2009, 74480H.

[10] K. D. Joensen, P. Hoghoj, F. E. Christensen et al., "Multilayered supermirror structures for hard x-ray synchrotron and astrophysics instrumentation," in *Multilayer and Grazing Incidence X-Ray/EUV Optics II*, vol. 2011 of *Proceedings of SPIE*, pp. 360–372, July 1993.

[11] L. Golub, G. Nystrom, E. Spiller, and J. Wilczynski, "Construction of multilayered X-ray telescope for solar coronal studies from space," in *Application of Thin-Film Multilayered Structures to Figured X-ray Optics*, vol. 563 of *Proceedings of SPIE*, pp. 266–275, 1985.

[12] E. Spiller and L. Golub, "Fabrication and testing of large area multilayer coated x-ray optics," *Applied Optics*, vol. 28, no. 14, pp. 2969–2974, 1989.

[13] M. Wohlschlägel, T. U. Schülli, B. Lantz, and U. Welzel, "Application of a single-reflection collimating multilayer optic for X-ray diffraction experiments employing parallel-beam geometry," *Journal of Applied Crystallography*, vol. 41, no. 1, pp. 124–133, 2008.

[14] P. Gawlitza, S. Braun, S. Lipfert, and A. Lesen, "Ion beam sputter deposition of x-ray multilayer optics on large areas," in

*Advances in X-Ray/EUV Optics, Components, and Applications*, vol. 6317 of *Proceedings of SPIE*, San Diego, Calif, USA, August 2006, 63170G.

[15] H. Tsuruta, S. Brennan, Z. U. Rek, T. C. Irving, W. H. Tompkins, and K. O. Hodgson, "A wide-bandpass multilayer monochromator for biological small-angle scattering and fiber diffraction studies," *Journal of Applied Crystallography*, vol. 31, no. 5, pp. 672–682, 1998.

[16] R. Dietsch, Th. Holz, D. Weißbach, and R. Scholz, "Large area PLD of nanometer-multilayers," *Applied Surface Science*, vol. 197-198, pp. 169–174, 2002.

[17] M. Nayak, P. N. Rao, and G. S. Lodha, "Magnetron sputtering based X-ray multilayer deposition system at Indus SR facility," *Asian Journal of Physics*, vol. 19, no. 2, pp. 1–14.

[18] R. V. Nandedkar, K. J. S. Sawhney, G. S. Lodha et al., "First results on the reflectometry beamline on Indus-1," *Current Science*, vol. 82, no. 3, pp. 298–304, 2002.

[19] L. G. Parratt, "Surface studies of solids by total reflection of X-rays," *Physical Review*, vol. 95, no. 2, pp. 359–369, 1954.

[20] Y. G. Shen, Y. W. Mai, Q. C. Zhang, D. R. McKenzie, W. D. McFall, and W. E. McBride, "Residual stress, microstructure, and structure of tungsten thin films deposited by magnetron sputtering," *Journal of Applied Physics*, vol. 87, no. 1, pp. 177–187, 2000.

[21] R. R. Kola, D. L. Windt, W. K. Waskiewicz et al., "Stress relaxation in Mo/Si multilayer structures," *Applied Physics Letters*, vol. 60, no. 25, pp. 3120–3122, 1992.

[22] S. Yulin, T. Feigl, T. Kuhlmann et al., "Interlayer transition zones in Mo/Si superlattices," *Journal of Applied Physics*, vol. 92, no. 3, pp. 1216–1220, 2002.

[23] R. F. Bunshah, *Handbook of Deposition Technologies for Films and Coatings*, chapter 5, Noyes Publications, 1994.

[24] E. Louis, A. E. Yakshin, P. C. Gorts et al., "Progress in Mo/Si multilayer coating technology for EUVL optics," in *Emerging Lithographic Technologies IV*, vol. 3997 of *Proceeding of SPIE*, pp. 406–411, February 2000.